To be published in Optics Express:

Title:	Photonically-Driven Pseudo-Continuous and Broadband THz Phase Shifting using Spatially-Resolved Photoconductivity Modulation
Authors:	Peizhao Li,Bowen Zheng,Jeffrey Hesler,Robert Weikle, II,Chao Gu,hualiang zhang,Lei Liu
Accepted:	27 July 25
Posted	01 August 25
DOI:	https://doi.org/10.1364/OE.570255

Photonically-Driven Pseudo-Continuous and Broadband THz Phase Shifting using Spatially-Resolved Photoconductivity Modulation

PEIZHAO LI,[1] BOWEN ZHENG,[2] JEFFREY L. HESLER,[3] ROBERT M. WEIKLE, II,[4] CHAO GU,[5] HUALIANG ZHANG,[2] AND LEI LIU[1,*]

[1]*Department of Electrical Engineering, University of Notre Dame, Notre Dame, IN 46556, USA*
[2]*Department of Electrical & Computer Engineering, University of Massachusetts Lowell, Lowell, MA 01854, USA*
[3]*Virginia Diodes Inc, Charlottesville, VA, 22902, USA*
[4]*Department of Electrical & Computer Engineering, University of Virginia, Charlottesville, VA 22904, USA*
[5]*Centre for Wireless Innovation, Electrical Engineering and Computer Science, Queen's University Belfast, Northern Ireland, BT3 9DT, UK*
**lliu3@nd.edu*

Abstract: We report a novel and unique approach for achieving high-performance and broadband THz phase shifting based on spatially-resolved photoconductivity modulation (SRPM). By changing the illumination area on a hybrid Au-Ge mesa-array (AGMA) structure in front of an indium tin oxide (ITO) layer for local photoconductivity modulation, the phase difference between the incident- and reflected-waves can be tuned nearly continuously with extremely low reflection loss. For a prototype demonstration, a photonically-driven THz phase shifting device based on the WR-5.1 (140-220 GHz) waveguide configuration was designed, modeled and simulated. To achieve phase tuning in the range of 0° to -180° at 180 GHz (band center frequency), a mesa-array consisting of 12 x 6 unit cells (each 105 μm × 105 μm) was designed, and a distance *d* of 250 μm between the AGMA and ITO was used. The SRPM is accomplished using computer-generated light patterns from a closely-coupled micro-LED array for through-ITO illumination, without the need for any biasing circuitry. Full wave simulation results have shown that pseudo-continuous and broadband phase shifting can be achieved in the entire WR-5.1 band, and a shifting range of 0° to -180° at 180 GHz can be realized as designed. In addition, by using light patterns of different combinations of vertical strips, a fine phase tuning step as small as ~0.05° can be demonstrated. For all phase tuning states, the simulated reflection loss is generally less than 1 dB with low loss variation. The proposed technology for high-performance THz phase modulation is promising and powerful, while offering far more design flexibility and frequency scalability than the current state-of-the-art since it requires no biasing wires thus eliminating parasitic-related performance degradation. Therefore, this technology is suitable for the development of large-scale THz phased-arrays, reconfigurable reflectarrays, and tunable metasurfaces for dynamic beam steering/forming required in next generation (6G or beyond) wireless communications.

1. Introduction

The rapid development of wireless communication technologies has led to a significantly increased demand for enhanced data transmission capabilities, such as higher data rate, higher bandwidth, improved reliability etc. [1]. Therefore, there is growing interest in exploring higher-frequency bands such as THz, which broadly extends from 100 GHz to 10 THz [2]. The sub-THz band is of particular interest for 6G (e.g., the bands centered at 170 GHz, and 300 GHz) and future-G wireless communications. This sub-THz frequency spectrum holds substantial potential for dramatically enhancing communication performance, as it provides extensive unused bandwidth that can significantly boost data transmission, minimize latency,

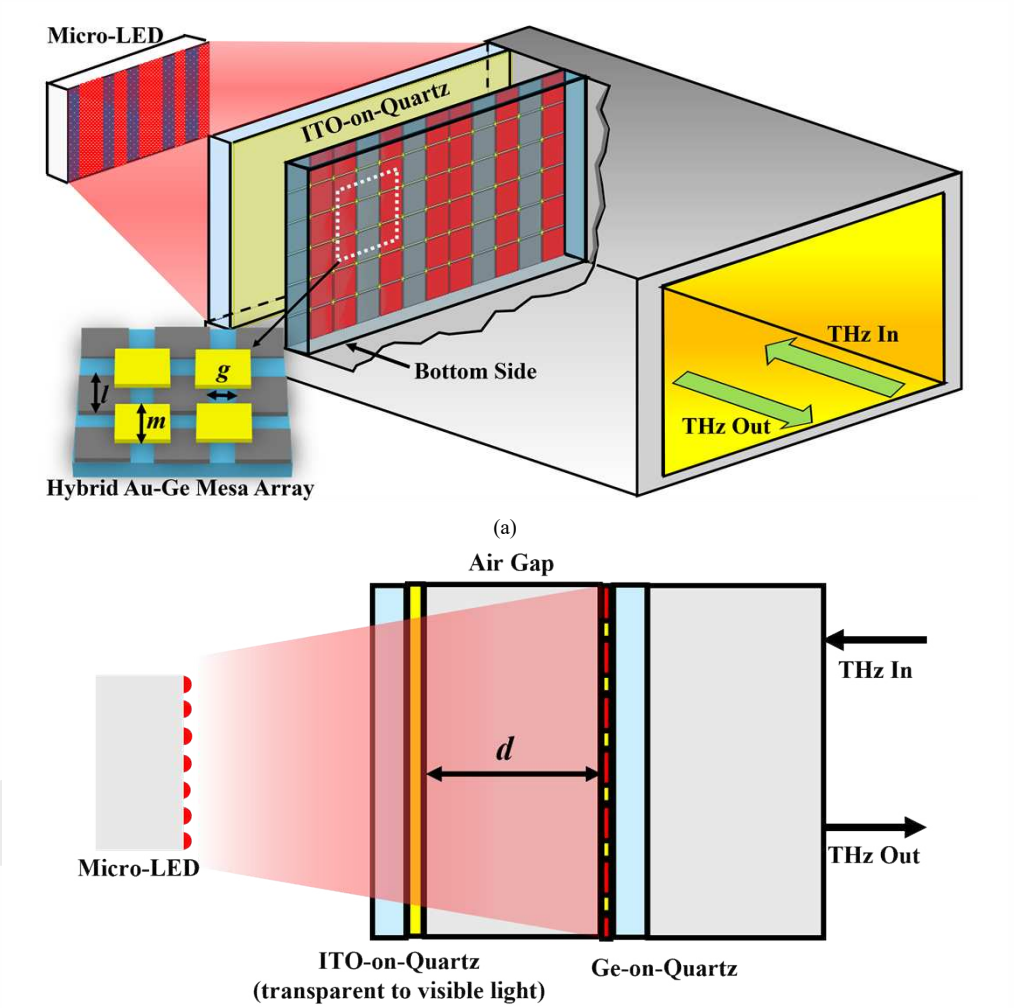

Fig. 1. (a) The conceptual design of the THz phase shifting device based on WR-5.1 waveguide configuration using SRPM in a hybrid Au-Ge mesa array (AGMA) structure, and (b) the cross-section view of the proposed phase shifting device with a quartz/ITO/air/AGMA/quartz device configuration (ITO is employed since it allows controlling light signal to pass while presenting high reflectivity for the incident THz waves).

and accommodate a large number of concurrently connected devices [3]. However, due to the limited available THz power (i.e., the THz gap) and severe path loss (due to shorter wavelengths and strong atmosphere absorption), a dynamic high-gain directional transmission/radiation THz beam with narrow beamwidth is highly desired [4] in such communication links. As a result, dynamic THz beam steering and forming technologies have attracted much attention and become essential for emerging applications in the next generation communication such as augmented reality (AR), virtual reality (VR), high-definition multimedia streaming, and Internet of Things (IoT) connectivity [5].

In order to achieve efficient THz beam steering and forming, an essential technology required in many systems especially those employing phased-array antennas and reflectarrays, is THz phase shifting. Tunable and reconfigurable phase shifters are critical elements responsible for accurate beam steering/forming for enabling targeted transmission and reception of signals [6]. Although various technologies have been explored for phase shifting at microwave and millimeter-wave frequencies [7]-[13], these approaches have not yet been

viable for THz frequencies. First, traditional semiconductor-device-based phase shifting using PIN diodes, switches (e.g., HEMTs) and varactors [7]-[9] suffer significant performance degradation at THz bands due to increased parasitic effects, reduced carrier mobility, and stringent device scaling requirements at micrometer or sub-micrometer dimensions. Meanwhile, MEMS-based phase shifters [10], while offering advantages such as low insertion loss and high linearity, face substantial challenges in terms of device reliability, slow tuning speed, fabrication repeatability, and complex manufacturing processes, especially when being integrated into high-frequency large-scale phased-array or reflectarray systems. Moreover, phase shifters based on tunable materials such as graphene, VO_2, and liquid crystals (LCs) have also been proposed and explored [11]-[13], but they rely on inconvenient modulation using high voltage, orientation of LC, or temperature change, respectively, making them challenging to be integrated into large-scale and complex THz systems. In addition, most aforementioned devices typically operate in only two discrete states making them unsuitable for applications requiring continuous phase control. Finally, all the above phase shifting technologies require external biasing circuits for tuning devices which introduces parasitic-related performance deterioration, increases circuit complexity and complicates system integration, especially as operating frequencies approach the THz range.

To overcome the above limitations, for the first time, we propose an alternative and unique approach utilizing spatially-resolved photoconductivity modulation (SRPM) [14]-[15] in semiconductor materials to achieve high-performance phase control at THz frequencies. The approach is based on changing the illumination area of a hybrid Au-Ge mesa-array (AGMA) structure in front of an indium tin oxide (ITO) layer for local photoconductivity modulation, thus optically tuning the incident THz wave effective reflection plane for producing relative phase shifting. For a prototype demonstration, a THz phase shifting device based on a WR-5.1 waveguide configuration is designed, analyzed and simulated. Although the proposed approach can also be used for designing free-space quasi-optical phase shifting elements (e.g., unit cells in a reflectarray or metasurface), this waveguide demonstration allows us to verify the proposed concept, validate the design methodology, and evaluate the achievable device performance using convenient full-wave simulations and well-established experimental setup (e.g., WR-5.1 waveguide vector network analyzer (VNA) extenders and calibration procedures (e.g., TRL, SOLT, etc.)). As shown in Fig. 1, the proposed device consists of a hybrid AGMA structure (on a thin quartz substrate) encapsulated within a WR-5.1 waveguide with one end loaded by an ITO-on-Quartz substrate (as the "ground" for low loss THz reflection). The mesa-array layer and the ITO are separated by air with a distance of *d* (for determining the phase tuning range), forming a Quartz/ITO/air/AGMA/Quartz (QIAAQ) device configuration. A closely-coupled micro-LED array is placed at the backside for through-ITO illumination (as ITO and quartz are transparent to visible light) for local photoconductivity modulation in Ge (in the mesa-array). By using computer-generated light patterns with different combinations of vertical strips, the illumination area on the mesa-array can be tuned, leading to variable effective reflection plane for phase shifting. Full-wave simulation using HFSS was performed to demonstrate the potential of the proposed technology. The simulation has shown that the proposed approach offers superior THz phase shifting performance as compared to competing technologies, including nearly continuous phase tuning, wide tuning range (0°-360° achievable), extremely low reflection loss, low loss variation, and broadband operation. Additionally, the proposed technology requires no biasing circuitry, making it suitable for employment in THz phased-arrays, large-scale reflectarrays, and metasurfaces for dynamic beam steering/forming required in next generation wireless communications.

2. Physics-Based Modeling of Spatially-Resolved Photoconductivity Modulation in Semiconductor

When a semiconductor is illuminated by light, electrons in the valence band can be excited to the conduction band as long as the provided photon energy exceeds the semiconductor's

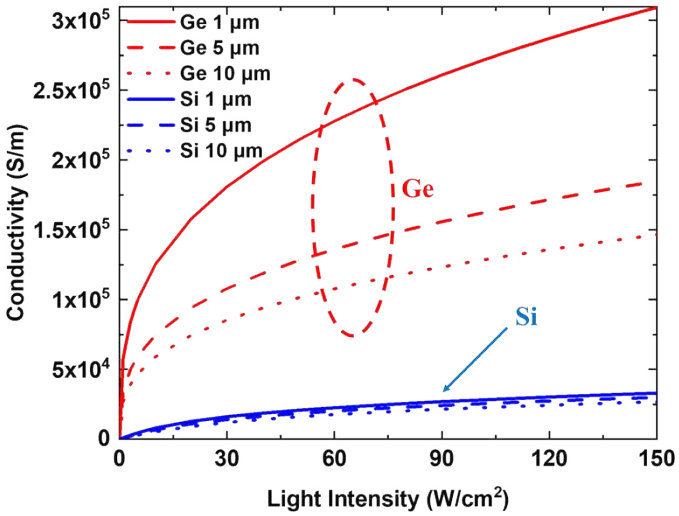

Fig. 2. The photoconductivity of Si and Ge films as a function of light intensity for different film thicknesses.

bandgap, thereby generating free carriers (i.e., electrons and holes). The concentration n of these photoinduced free carriers is influenced by various factors, including the wavelength (or angular frequency ω), intensity of the incident light P (assume normal incidence along the z-direction), as well as intrinsic properties of the semiconductor material. Mathematically, this relationship can be expressed using the following 1-D continuity equation and boundary conditions as [16]:

$$D_n\frac{d^2n}{d^2} + \frac{\alpha P(1-R)}{\hbar\omega}e^{-\alpha z} - \frac{n}{\tau_{eff}} = 0 \quad (1)$$

$$D_n\frac{dn}{dz}|_{z=0} = D_n\frac{dn}{dz}|_{z=H} = V_{SR} \quad (2)$$

where D_n represents the diffusion coefficient, α is the absorption coefficient, R is the surface reflectivity, $\hbar$ is Planck's constant, τ_{eff} is the effective carrier lifetime, H is the semiconductor thickness along the z-direction, and V_{SR} is the surface recombination velocity. For semiconductors under strong light illumination, Auger recombination becomes one of the dominant effects that determine the effective carrier lifetime (and hence the achievable photoconductivity) under high carrier concentration (e.g., >~10^{18} cm^{-3} in Si). Therefore, the τ_{eff} of a semiconductor including Auger recombination can be expressed by,

$$\frac{1}{\tau_{eff}} = \frac{1}{\tau_{bulk}} + \gamma n^2, \quad (3)$$

where τ_{bulk} is the bulk semiconductor carrier lifetime, and γ is the Auger recombination coefficient (e.g., γ_{Si} = 3×10^{-31} cm^6/s, and γ_{Ge} = 1×10^{-31} cm^6/s). Once the carrier concentration can be optically modulated, the resulting photoconductivity σ of the semiconductor material can then be locally modulated following $\sigma = q\,(\mu_n + \mu_p)\,n$, where q is the elementary charge, μ_n and μ_p are the effective electron and hole mobilities, respectively. Once again, both the electron and hole mobilities in the above equation are functions of carrier concentrations, and this effect becomes more significant when concentrations are high (e.g., >~10^{17} cm^{-3} in Ge). For example, in Ge, the carrier mobilities are empirically proportional to $1/(1+n/10^{17})^{0.5}$ [17].

From the above discussion, it is seen that the effective carrier lifetime of the semiconductor material is one of the key parameters that determines the photoconductivity modulation. Longer lifetime leads to higher achievable photoconductivity while unavoidably resulting in lower modulation speed [15],[18]-[19]. Taking Si and Ge as examples and assuming well surface passivation (V_{SR}=0), the achievable photoconductivities have been calculated for different light

intensities (P=0-150 W/cm^2) and semiconductor thin-film thicknesses (H), as shown in Fig. 2. The incident light wavelength was assumed to be 750 nm (i.e., red, can be generated by commercially available micro-LEDs) for a prototype demonstration. It is seen that the photoconductivity increases rapidly with light intensity initially and then saturates as the illumination intensity increases further. This is a consequence of both significant Auger recombination and reduced carrier mobilities when the carrier concentration is relatively high (~10^{18} cm^{-3}) [17], [20]. For both Si and Ge, thinner films show higher carrier concentration and hence high photoconductivity under the same light intensity (assuming no significant surface carrier recombination as the Si and Ge are fully passivated [16]). In addition, Ge thin films generally present higher photoconductivity than Si under identical illumination intensities (assuming same film thickness) due to their longer carrier lifetime (e.g., 1 ms), relatively higher carrier mobility, larger light absorption coefficient (~5×10^5 cm^{-1}), and smaller Auger coefficient (1×10^{-31}cm^6/s). Specifically, for a light intensity of 120 W/cm^2 (where both Si and Ge start to "saturate"), photoconductivities of ~3×10^4 S/m and ~2.5×10^5 S/m can be achieved for 1 μm thick Si and Ge, respectively. As a result, Ge is more suitable for applications exploiting the huge transition from a low-loss dielectric state to highly-conductive state for THz wave modulation/manipulation. Therefore, Ge is chosen for photoconductivity modulation to realize high-performance THz phase shifting in the following study and investigation in this paper.

Although the above SRPM mechanism has already been explored and applied in demonstrations of a wide range of THz applications, including coded-aperture imaging [21], beam steering/forming antennas [22], waveguide attenuators [23]-[24], and switching devices [25]-[26], these implementations have exclusively relied on magnitude modulation of THz waves. To date, THz phase modulation using SRPM directly has never been reported or explored. To fully unlock the potential of the SRPM for THz wave manipulation and achieve high-performance THz phase modulation, we propose to explore and demonstrate the feasibility of producing phase shift in a reflective device by varying the illumination area on Ge for changing the effective reflection plane. However, this is particularly challenging since the typical carrier diffusion length in Ge (i.e., $\lambda_d = \sqrt{D_n \tau_{eff}}$ = ~2 mm) is already significantly larger than the wavelengths (e.g., 1 mm at 300 GHz) and dimensions of many devices for operation at THz frequencies. For example, the WR-5.1 (140-220 GHz) waveguide configuration to be employed for a prototype demonstration in this paper has a dimension of 1.2954×0.6477 mm^2, making it impossible to perform local photoconductivity modulation for achieving different conductive areas inside such a small device. Nevertheless, in such material as Ge, photo-induced carriers generated within the illuminated area tend to diffuse into adjacent areas, resulting in both low carrier concentration and hence achievable photoconductivity, as well as low spatial resolution of SRPM. Therefore, instead of using naturally-existing semiconductors such as Ge (or Si), a novel engineered photoconductive material that exhibits a large carrier lifetime for achieving high conductivity and yet short lateral diffusion length allowing high spatial resolution local photoconductivity modulation is urgently required. Such contradictory property does not exist in natural-existing materials but can be realized by a novel and unique mesa-array structure.

3. Hybrid Au-Ge Mesa-Array Structure

As discussed previously, in order to achieve both high photoconductivity (or modulation depth) and high spatial resolution for enhanced SRPM, a mesa-array structure consisting of a matrix of isolated and subwavelength islands can be used to restrict the lateral diffusion by confining photo-induced free carriers within a limited area determined by the mesa size. Using a Si mesa-array structure, THz coded-aperture imaging at 740 GHz with a subwavelength imaging resolution has been demonstrated [27]. In this demonstration, a matrix of Si mesas, each with a lateral dimension of 105×105 μm^2 and a trench width of 7 μm was employed. Small corner Si junctions were added to connect adjacent mesas (i.e., semi-isolated) for suppressing THz propagation through trench gaps while facilitating easy fabrication. However, due to the residue

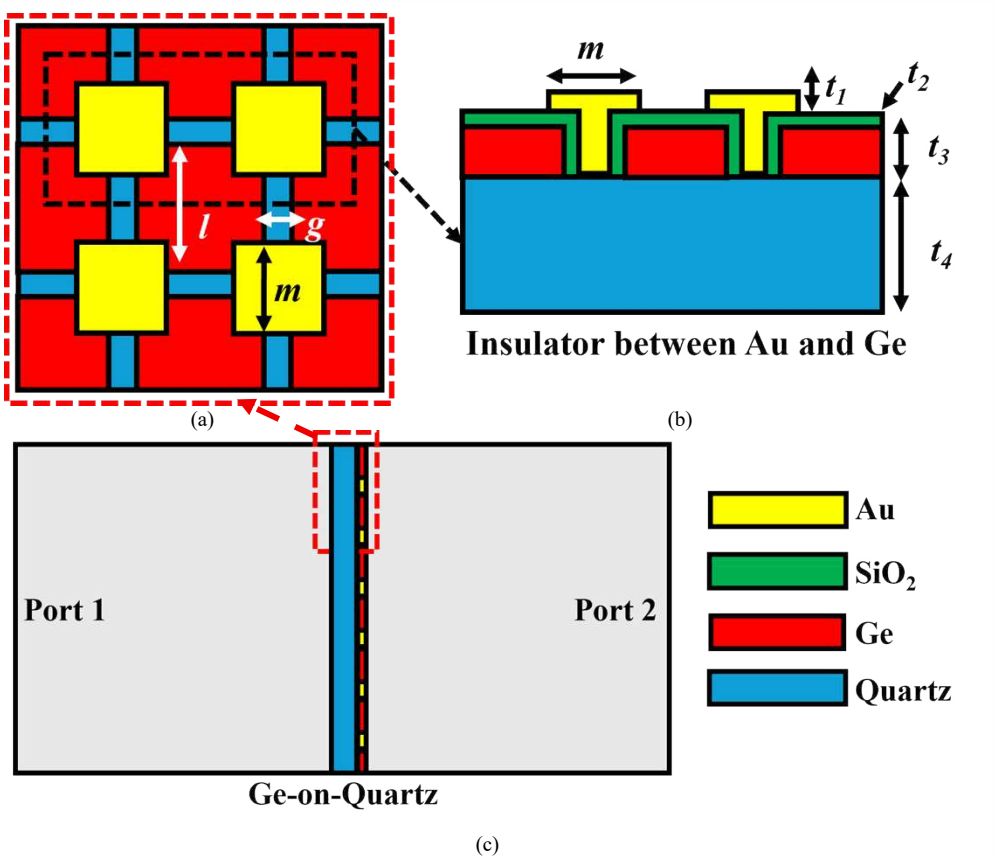

Fig. 3. (a) The top view and (b) cross-section view of the proposed hybrid AGMA structure; (c) the side view of the WR-5.1 configuration used to evaluate the SRPM performance using different mesa-array structures.

carrier diffusion through these corner junctions, an imaging resolution of only ~400 μm has been demonstrated, which is worse than the expected ~105 μm resolution determined by the mesa size. This issue becomes even more severe in Ge where the achievable imaging resolution is anticipated to be even worse (due to much longer diffusion length) by using the same mesa-array design, given that the carrier lifetime in Ge is more than 100 times longer than that in Si [15]. Consequently, the approach using the semi-isolated mesa-array is also unsuitable for high performance THz phase modulation using SRPM in Ge in a small WR-5.1 waveguide.

In order to address the above issue and to enable high performance SRPM with high spatial resolution in Ge for achieving efficient phase shifting in WR-5.1, we proposed to employ a hybrid AGMA structure as described in [28]. As illustrated in Fig. 3 (a), the AGMA comprises an array (trench size g=2 μm) of Ge mesas, each with a thickness of 5 μm and dimension of 105×105 μm^2 ($l \times l$), placed on a 50-μm-thick quartz substrate. The Ge mesa dimension was designed so that exactly 12 × 6 unit cells will be included inside the waveguide aperture for pseudo-continuous phase modulation with small tuning step, as a prototype demonstration later in this paper. The 2 μm trench was chosen to ensure high modulation depth (smaller gap preferred) while facilitating easy fabrication using traditional photolithography without using electron-beam lithography (EBL). In contrast to the semi-isolated mesa-array structure, the Ge mesas in this AGMA are fully isolated, while the small corner junctions are replaced by Au joints with a dimension of 10 um x 10 um ($m \times m$, i.e., 1 um-thick (t_1) Au cap on top of 5 μm-thick (t_3) Au embedded in Ge trench as shown in Fig. 3(b)). Once again, these Au joints act to suppress potential THz wave propagation through the trench gaps for achieving high modulation depth. Most importantly, to ensure that the Ge mesas are fully isolated, a 2-nm-

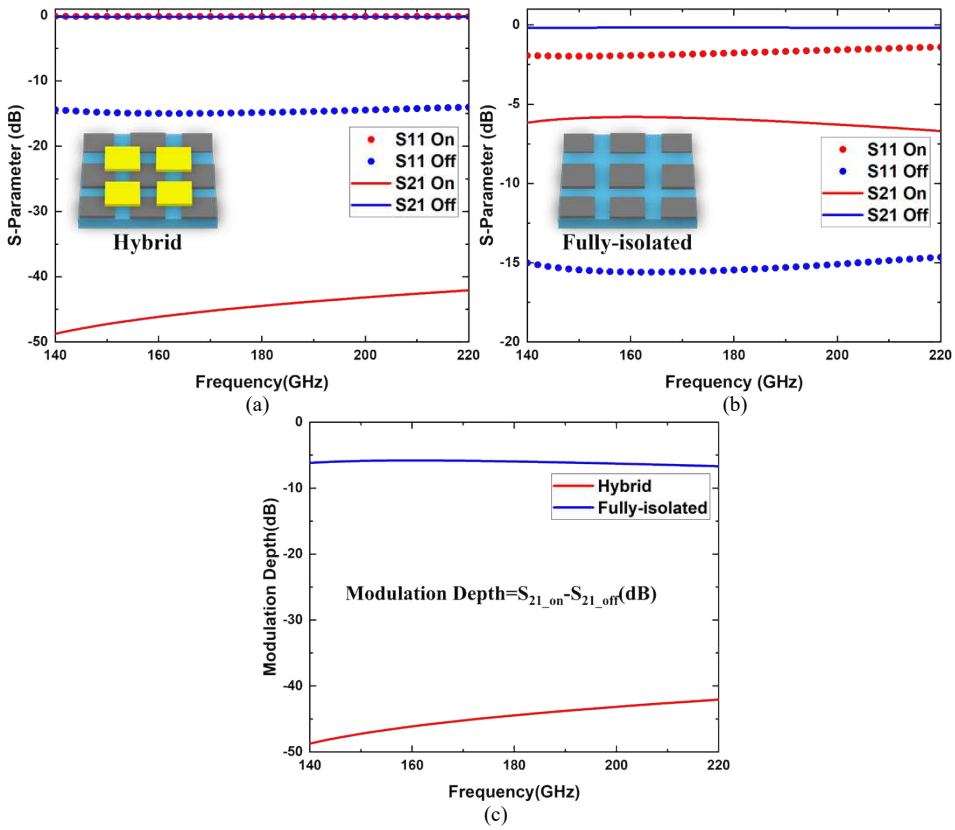

Fig. 4. Simulated two-port S-parameters for (a) the hybrid AGMA structure and (b) fully-isolated Ge mesa-array structure; (c) comparison of modulation depths ($D = S_{21\_on} - S_{21\_off}$ (dB)) achieved using the two structures.

thick (t_2) SiO_2 insulating layer is inserted between the Au joints and the Ge mesas as shown in Fig.3 (b). By introducing the Au joints and insulating layer between adjacent mesa elements, lateral carrier diffusion can be effectively suppressed. This structural modification (i.e., hybrid AGMA) directly results in much enhanced spatial resolution (now solely determined by the mesa size) as compared to the previous semi-isolated Si mesa-arrays while maintaining the capability of achieving very high photoconductivity using Ge. It is worth to point out that the implemented insulating layer not only prohibits lateral carrier diffusion but also acts as a surface passivation layer, substantially lowering the surface carrier recombination [29]. Finally, the proposed hybrid AGMA can be fabricated using a well-established process using reactive ion etching (RIE) for forming the Ge mesas (with photolithography), followed by atomic layer deposition (ALD) for insulation layer, and electron beam (E-beam) evaporation (followed by lift-off) to define the Au joints [26].

Building on the modified structure described earlier, a 12 × 6 hybrid AGMA was designed using a Ge (5 μm-thick) on quartz (50 μm-thick) (GoQ) substrate. Each mesa has a dimension of 105×105 μm^2, and the trench size is g=2 μm, following the design described above. To facilitate the WR-5.1 phase shifter design, the performance of the AGMA structure for SRPM was evaluated by placing it into a WR-5.1 waveguide for full-wave simulation using HFSS, as shown in Fig. 3(c). This configuration of 12 × 6 mesas (l =105 μm, g=2 μm) was designed to be accommodated inside the small WR-5.1 aperture (1.2954 mm by 0.6477 mm, see Fig. 3(c)) while allowing a high spatial resolution (i.e., 105 um, determined by the unit mesa size) to be achieved. Fig. 4 shows the simulated two-port S-parameters and the achieved modulation depths for the hybrid AGMA and fully-isolated Ge mesa-array (5 μm-thick Ge on 50 um-thick

quartz, 2 um trench gap, without corner junctions) placed inside the same WR-5.1 waveguide (as shown in Fig. 3(c)) for performance comparison. As shown in Fig.4 (a), under the non-illuminated condition (i.e., off-state), the hybrid AGMA exhibits a S_{11} of ~ -14 dB and S_{21} of 0.2 dB, indicating that nearly all of the THz power was transmitted from port 1 to port 2 due to the low loss Ge employed. Conversely, when fully illuminated (i.e., on-state) using a light intensity of 150 W/cm^2 (assuming a conductivity of 180,000 S/m for 5 μm-thick Ge as shown in Fig.2), the AGMA exhibits a S_{11} of -0.13 dB and an average S_{21} of approximately -45 dB within the frequency range of 140-220 GHz. This indicates that nearly all of the incident THz power was reflected back to port 1 because of the high photoconductivity achieved. For a comparison, Fig. 4 (b) shows the S-parameters for the fully-isolated Ge mesa-array structure without the Au joints. In the off-state, this structure exhibits an average S_{11} of -15 dB and S_{21} of -0.16 dB. However, in the on-state, an S_{11} of approximately -1.7 dB and an S_{21} of only -6 dB are observed, suggesting that a large amount of THz power was still transmitted to port 2 due to the THz wave propagation (or leakage) through the trenches. As a result, as shown in Fig. 4(c), the hybrid AGMA structure exhibits a much higher modulation depth (the difference between the on-state S_{21} and off-state S_{21}, i.e., $D = S_{21\_on} - S_{21\_off}$ (dB)) of ~45 dB, substantially exceeding the modulation depth of only ~6 dB observed in the fully-isolated mesa-array structure. This proves that the introduction of the Au joints effectively suppresses THz wave propagation through the trenches, enabling a much higher modulation depth to be achieved (while same time ensuring a higher spatial resolution determined by the unit mesa size). Overall, the comprehensive simulation and analysis performed in this section clearly demonstrates the effectiveness of the proposed hybrid AGMA structure for achieving enhanced SRPM.

4. Pseudo-Continuous Phase Shifter Design and Simulation

On the basis of the above hybrid AGMA design and simulation for enhanced SRPM, a prototype reflective THz phase-shifting device based on a single port WR-5.1 (140-220 GHz) waveguide configuration, and using the proposed approach is illustrated in Fig. 1(a). For a proof-of-concept demonstration, the device is designed with a goal to achieve 0° to -180° ("-" to emphasize phase delay) phase shifting between the incident and reflected waves at port 1 for the center frequency of 180 GHz, as shown in Fig. 5(a) inset. The device architecture incorporates an active component consisting of a 12 × 6 (N×M) hybrid AGMA placed on a 50 μm-thick quartz substrate (same as the device evaluated in section 3) for photoconductive modulation. The quartz substrate provides support for the thin AGMA structure, and thinner quartz (e.g., 20 μm or 10 μm) is preferred to further reduce partial THz refection at the interface and insertion loss through the substrate. In addition, a 1 μm-thick ITO layer (with a conductivity of ~2.8×10^6 S/m) deposited onto a thin quartz substrate is loaded at the waveguide end to serve as a conductive reflection plane ("ground") for low-loss THz reflection, while preserving the ground connection of the outer waveguide wall. The ITO-on-quartz substrate is optically transpartent allowing optical signals to pass for performing SRPM on the hybrid AGMA. The AGMA structure and ITO are separated by air with a distance of *d* (determines the achievable phase tuning range) to form a QIAAQ device configuration. Meanwhile a closely-coupled micro-LED array behind the ITO-on-quartz substrate is employed for spatially selective illumination (through ITO) on the AGMA for phase tuning. These micro-LEDs typically generate 400-800 nm visible light with a device area smaller than 5 μm × 5 μm [30]. They are capable of delivering an irradiance of around 822.4 W/cm² [31], significantly surpassing the light intensity (e.g., 100-150 W/cm^2) required in the proposed phase modulation scheme. For precise alignment between the micro-LED array and the AGMA, optics for focusing and careful alignment process are needed to guarantee that each Ge mesa can be individually controlled without affecting adjacent mesas for correct phase modulation by its corresponding light source.

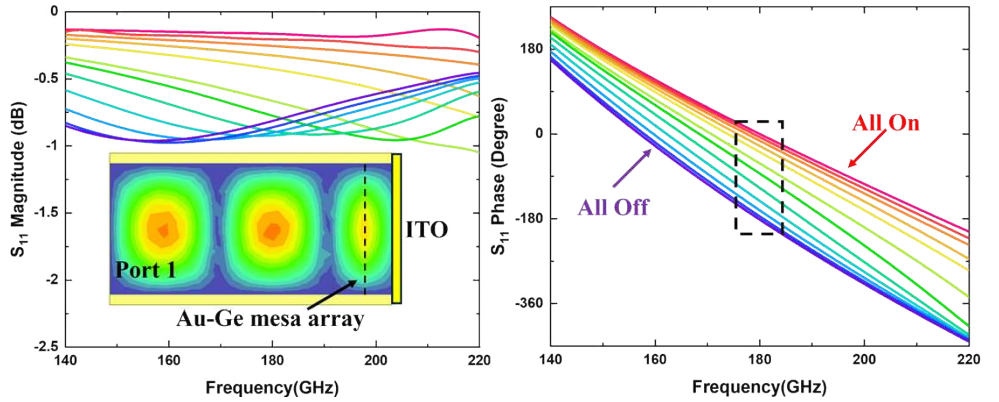

(a) (b)

Fig. 5. (a) Simulated S_{11} magnitude (inset: the top view of the electric field distribution at 180 GHz) and (b) S_{11} phase delay of the proposed device under different combinations of illuminated vertical mesa strips (phase delay normalized to the phase at 180 GHz for full illumination state (i.e., All-On).

The mechanism of THz wave phase modulation in the proposed device can be understood in terms of shifting the effective reflection plane (for the incident THz wave at port 1, see Fig. 5(a) inset). Under the non-illuminated (i.e., no light from the micro-LED array) condition, the AGMA behaves as a low loss material, and the incident THz wave can go through and get reflected from the conductive ITO surface, setting the reflection plane at the ITO/air interface (for maximum phase shift, i.e., -180° at 180 GHz). Conversely, full illumination of the AGMA shifts the effective reflection plane to the mesa-array/quartz interface (for minimum phase shift, i.e., 0° (phase delay) at 180 GHz), thus achieving a phase shifting with a tuning range determined by the separation distance d between the mesa-array and ITO layers. In this prototype demonstration, to achieve a -180° phase shift at 180 GHz, the device was designed with d = 250 μm. This distance is smaller than the quarter guided wavelength of 545 μm for the WR-5.1 waveguide at 180 GHz, due to the fact that the effective guided wavelength (for the wave between the mesa-array and ITO) being shortened by the hybrid AGMA structure and the 50 μm-thick quartz substrate (see Fig. 5(a) inset).

Furthermore, in addition to the maximum (all off) and minimum (all on) phase shifting, nearly-continuous phase modulation can be realized by selectively changing the illumination area on the hybrid AGMA layer. To verify this approach, full-wave simulations were performed for the proposed THz phase-shifting device by illuminating light patterns with different combinations of vertical mesa-array strips (total N=12 strips/columns). It is well known that for a periodic grating structure with a pitch size (P, or grating slit spacing) equal or larger than the wavelength (λ), diffraction (with a diffraction angle θ) will happen following the equation $\sin(\theta) = m(\lambda/P)$, where m is the diffraction order. However, in our phase shifting approach and the prototype waveguide design using a hybrid AGMA array, the unit cell (or single mesa) or the vertical strip width is purposely chosen to be well below wavelength. For example, at 180 GHz (the center of WR-5.1), the guided wavelength in air is 2.18 mm, and the guided wavelength in quartz is approximately 1.1 mm. The waveguide aperture has a dimension of 1.2954 × 0.6477 mm^2 with 12×6 unit cells, so each unit cell (~105 μm) is roughly 1/21 wavelength (or ~1/11 wavelength in quartz). Therefore, for all tuning patterns to be used, and following the above diffraction equation, λ should be much larger than P, and the diffraction effects have been minimized. Fig. 5(a) presents the simulated reflection coefficient (S_{11}) magnitudes for illumination with selected representative light patterns (each strip can be turned "on" or "off"). It can be observed that the reflection loss generally remains below 1 dB for the entire G-band (140 GHz to 220 GHz) with a low loss variation of < 0.9 dB. Additionally, Fig. 5(b) shows the simulated relative phase shift (i.e., phase normalized to the minimum phase shift

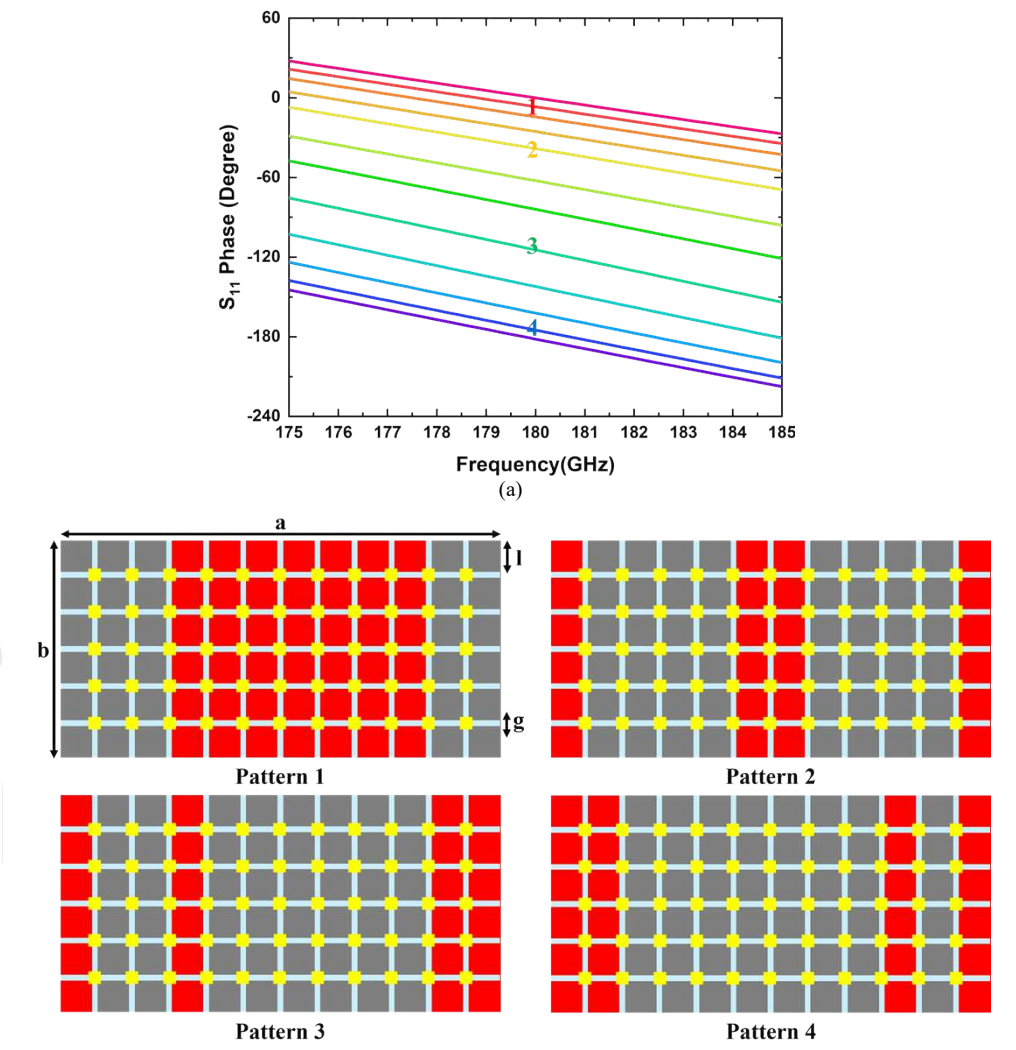

Fig. 6. (a) Zoomed-in view of phase shifting within the frequency range of 175-185 GHz, and (b) the illumination patterns corresponding to the cases labeled in (a). (Dimensions: a = 1.2954 mm, b = 0.6477 mm, *l*=105 μm, and g = 2 μm.)

at 180 GHz) demonstrating that as the illumination area gradually decreases (i.e., transitioning from "all on" to "all off"), the phase shift consistently increases across the entire G-band. Therefore, the simulation results verify that the effective reflection plane can be effectively adjusted from the hybrid AGMA plane to the ITO plane leading to broadband (i.e., 140 GHz to 220 GHz) phase modulation of THz wave using the proposed approach. Although the phase shifting varies with frequency, the results in Fig. 5(b) indeed shows the broadband operation property since the proposed approach is based on true-time-delay of wave propagation [32].

In order to verify the design strategy, Fig. 6 (a) shows a zoomed-in view of the phase shifting within the frequency range of 175 GHz to 185 GHz (highlighted in Fig.5 (b) using dashed rectangle). Specifically, the relative phase shift at 180 GHz changes exactly from 0° to -180° as designed by using an ITO-to-AGMA distance of *d*=250 μm. A larger and arbitrary phase tuning range (e.g., 0-360°) can be easily achieved by using a different ITO-to-AGMA distance. To further investigate the phase tuning capability using different illumination light patterns,

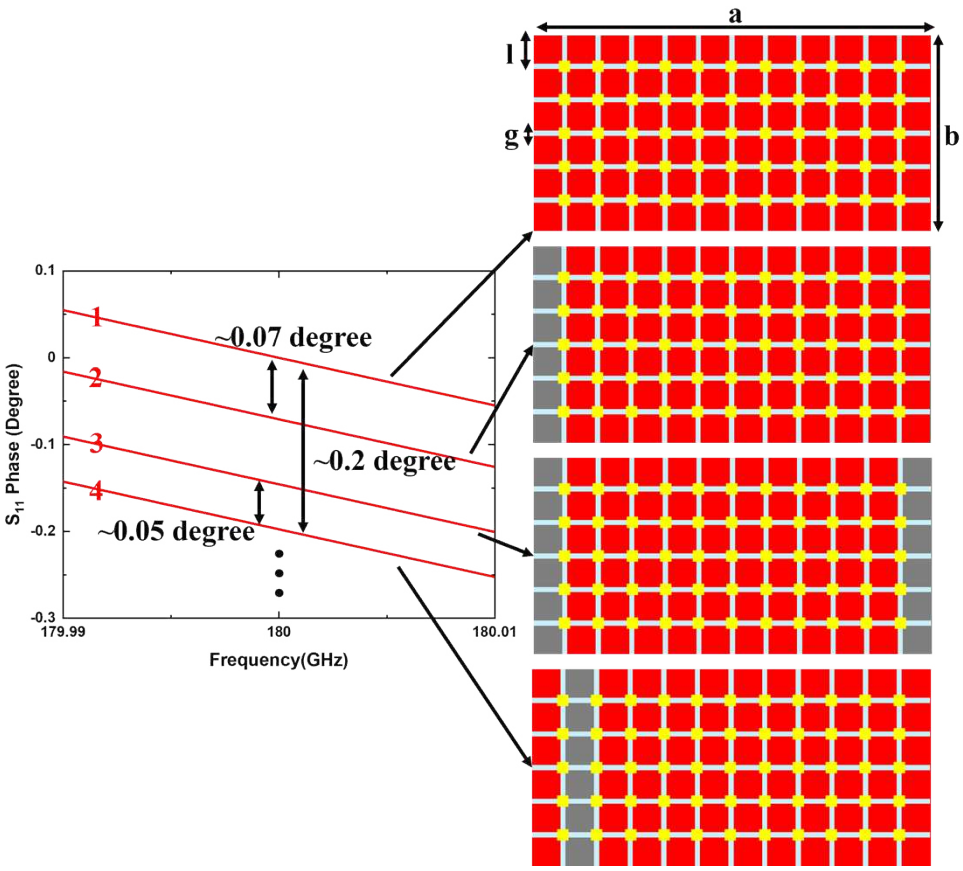

(a) (b)

Fig. 7. (a) Demonstration of phase fine-tuning capability, and (b) corresponding illumination patterns (from top to bottom) associated with each phase state. (Dimensions: a = 1.2954 mm, b = 0.6477 mm, *l*=105 μm, and g = 2 μm.)

four distinct and representative phase-shifting responses in Fig. 6(a) are labeled as 1, 2, 3, and 4 for light pattern illustration. Since there are N=12 Ge mesa strips and each can be individually turned "on" and "off", there will be a total of 2^N light patterns that can be used. These 4 selected patterns are simply picked from a large number of different patterns for illustration and demonstration. As shown in Fig. 6(b), the light patterns resulting in phase shifting 1-4 are illustrated as Pattern 1-4, respectively. In these patterns, the red mesa regions indicate illuminated areas, whereas gray mesa regions represent areas without illumination. It is evident that illuminating the center region of the WR-5.1 waveguide induces significantly greater phase shifting compared to illuminating the mesa strips located at the edges. This is due to the intrinsic sinusoidal electric field (E-field) distribution within the rectangular waveguide, where the electric field is stronger in the center (of the longer side) than that near the sidewalls. Specifically, in this demonstration, turning "on" and "off" the AGMA columns at both edges yields the minimal phase shifting of ~0.07°, while modulating each of the two center strips results in substantial phase shifting of ~60°. This observation further suggests that fine-tuning of the phase shifting can potentially be achieved by adjusting the illumination patterns on the AGMA, especially by engaging the peripheral mesa strips.

To demonstrate the fine-tuning capability of the proposed approach using SRPM for THz wave phase modulation, Fig. 7(a) shows an example to achieve phase fine-tuning at 180 GHz. The phase shifts are associated with the four illumination patterns displayed in Fig. 7(b), in

sequential order from top to bottom. It can be observed that when all the mesas are illuminated, the phase shift produced is 0° as expected. In order to change the phase shift from 0° to -0.07°, the mesa strip on the left have to be "turned off", or not illuminated. Further turning off the light for the mesa strip on the right side results in the phase shifting from -0.07° to ~ -0.15°. Moreover, turning off only the second strip on the left produces a phase shift of ~ -0.2°, demonstrating a tuning step ($\Delta\theta$) as small as ~0.05° (between line 3 and 4 as seen in Fig.7 (a)). By employing various such combinations of mesa strip illumination (N=12 strips), mathematically $2^{N-1}+1 = 2^{11}+1 = 2049$ (considering that those vertical mesa strips and also the E-field are symmetrical about the waveguide center, e.g., N=1, 2 states; N=2, 3 states; N=3, 5 states; N=4, 9 states; N=5, 17 states… between 0° and -180°.) different phase tuning states can be achieved, leading to nearly continuous phase shifting across the range of 0° to -180° with a small tuning step of approaching 0.05°. When N is large, the phase tuning step can be approximately estimated following $\Delta\theta \approx 180^{\circ}/2^{N-1}$. Therefore, these results successfully confirm that the proposed technology using SRPM can achieve pseudo-continuous phase shifting by adjusting the illumination area on the hybrid AGMA structure.

Although the phase shifting device proposed here has been initially demonstrated and simulated using a WR-5.1 waveguide configuration in which angle of incidence is not a problem, the device can be also employed in free space as a unit cell for THz reflectarrays or metasurfaces. For these cases, the THz waves could be incident at different angles (not limited to normal incidence). Since the phase shifting device is based on adjusting the effective reflection plane, or in other words, the so-called true-time-delay of wave propagation, the fundamental working mechanism still holds well for oblique incidence. Therefore, for oblique THz wave incidence, the incident wave will be simply reflected following Snell's Law of reflection (i.e., reflection angle equals the incident angle, imagine an adjustable or movable reflection plane), with a phase shift slightly larger (due to longer path) than the designed value for normal incidence. In addition, since the device can dynamically and nearly-continuously tune the phase, the required phase shift for certain reflectarray or metasurface applications (e.g., 0°/180° for 1-bit beam steering/forming) can always be achieved. This is a unique advantage as compared to other phase-sifting unit cell design approaches. Initial full-wave simulation of a 50×50 reflectarray using the proposed phase shifting device as unit cells (i.e., oblique incidence for edge units), and fed by a small horn antenna for operation at 300 GHz has shown promising beam steering and forming performance, verifying that oblique incidence is not a significant issue affecting the deployment of the proposed device in practical applications.

5. Discussion

From the previous analysis, simulation and demonstration, it is seen that the proposed THz phase shifting technology using SRPM can deliver superior performance including nearly continuous phase shifting, large and arbitrary tuning range, extremely low reflection loss and low loss variation. While efficient phase shifting has been demonstrated using light patterns with different combinations of 12 vertical mesa strips, much more tuning states can be achieved by independently modulating all 12×6 (N×M) individual mesa units (i.e., using clusters of Ge mesas for different illumination areas, and ~ $2^{N\times M-2}$ (symmetrical field configuration about the waveguide center) phase shifting states can be achieved, leading to much smaller phase tuning steps. In addition, AGMA structures with more mesa units (e.g., N×M = 24×12 or much more (120×60 possible), determined by the controlling light wavelength) can be employed to enable pseudo-continuous and arbitrary phase modulation across the full 0°–360° range (by optimizing the ITO-to-AGMA distance *d*), directly addressing the critical limitation of discrete states (typically binary, 1 bit or 2 bits) associated with many other traditional phase shifting technologies employing MEMS, HEMTs, and PIN diodes. The proposed approach also significantly reduces reflection loss to less than 1 dB with a loss variation smaller than 0.9 dB, across the entire frequency band (and for all phase tuning states). This improvement is attributed to the high photoconductivity achieved using the hybrid AGMA structure and the

elimination of biasing circuits by employing the optical control technology. This level of phase modulation capability using the proposed approach has not been previously reported in the literature, and is prohibitively difficult to achieve using other competing technologies. It is worth to point out that the misalignment between the micro-LED array and the AGMA structure may introduce very small phase shift errors (e.g., <5% error, assuming the adjacent mesa(s) can be partially illuminated and modulated due to misalignment) determined by the ratio between the unit LED dimensions (e.g., 5 μm) and the Ge mesa size (e.g., 105 μm in this paper). This error can be further reduced by employing high quality micro-LED arrays with smaller unit LED dimensions. In addition, this small phase tuning error can be always compensated using our approach for nearly-continuous phase modulation, and won't significantly affect the practical applications of the proposed device (e.g., in a large-scale reflectarray).

Beyond the superior phase shifting performance achieved, the proposed approach using SRPM in a hybrid AGMA also offers broadband operation, enabling the device to support multi-band or frequency-agile THz systems without the need for redesign or reconfiguration. It is worth noting that the operation speed of the proposed phase shifting technology is primarily determined by the carrier lifetime in Ge in the hybrid AGMA structure [15]. Although Ge is chosen for the prototype demonstration in this paper owing to its high achievable photoconductivity, the relatively longer lifetime results in potentially lower modulation speed. Although other semiconductor materials could be used for higher speed, surface engineering during the RIE process for Ge mesa etching could be performed for controlling the surface carrier recombination to achieve relatively shorter lifetime and higher speed [26]. However, a short lifetime unavoidably leads to lower achievable carrier concentration and hence photoconductivity, therefore a trade-off between modulation speed and reflection loss has to be made for designing such THz phase shifting devices using the proposed SRPM technology.

In addition to superior performance and unique properties, the proposed THz phase shifting using SRPM technology also offers several advantages in terms of design flexibility and frequency scalability. First, although the proposed phase shifting was initially demonstrated using a single-port waveguide configuration, a THz circulator or coupler circuit could be adopted to separate the input and output for realizing a 2-port phase shifter component [33]-[34]. Such waveguide phase shifters can find practical applications in many THz phased-array antenna systems. In addition to waveguide configuration, the proposed QIAAQ device configuration could be also adopted as a unit cell design in a large-scale (e.g., 100×100 elements) metasurface or reflectarray for producing 2D arbitrary phase profiles for THz beam steering/forming as well as THz data link bending/curving. Second, as compared to all the other technologies, the proposed approach accomplishes phase shifting by optical control without the need for any biasing circuitry. This eliminates any parasitic-related performance degradation making the proposed approach not only readily scalable to higher THz frequencies (e.g., > 300 GHz), but also suitable for developing large scale reflectarrays or metasurfaces for next generation THz wireless communications.

6. Conclusion

A novel, unique and powerful technology for achieving high-performance and broadband THz phase shifting has been proposed. This approach is based on local photoconductivity modulation in a hybrid AGMA structure to produce different conductive areas for reflective phase shifting. For a prototype demonstration, a photonically-driven THz phase shifting device using the WR-5.1 waveguide configuration was designed, modeled, and simulated. Simulation results show that pseudo-continuous and broadband phase shifting in the entire 140-220 GHz can be achieved, with large tuning range, extremely low reflection loss, small loss variation and refined tuning steps. The proposed THz phase shifting technology based on spatially-resolved photoconductivity modulation is promising for the development of large-scale THz phased-arrays, reconfigurable reflectarrays, and tunable metasurfaces for dynamic beam steering/forming required in next generation (6G or beyond) wireless communications.

Funding. National Science Foundation (ECCS-2223949)

Disclosures. The authors declare no conflicts of interest

Data Availability. Data underlying the results presented in this paper are not publicly available at this time but may be obtained from the authors upon reasonable request.

References

1. Z. Ma, M. Xiao, Y. Xiao, Z. Pang, H. V. Poor, and B. Vucetic, "High-reliability and low-latency wireless communication for Internet of Things: challenges, fundamentals, and enabling technologies," IEEE Internet Things J. 6, 7946–7970 (2019).
2. H.-J. Song and N. Lee, "Terahertz communications: challenges in the next decade," IEEE Trans. Terahertz Sci. Technol. 12, 105–117 (2022).
3. J. M. Jornet et al., "The Evolution of Applications, Hardware Design, and Channel Modeling for Terahertz (THz) Band Communications and Sensing: Ready for 6G?," in Proceedings of the IEEE
4. R. Xu, S. Gao, B. Sanz Izquierdo, C. Gu, P. Reynaert, and A. Standaert, "A review of broadband low-cost and high-gain low-terahertz antennas for wireless communications applications," IEEE Access 8, 57615–57629 (2020).
5. J. Chakareski, M. Khan, and M. Yuksel, "Toward enabling next-generation societal virtual reality applications for virtual human teleportation: a novel future system concept and computation-communication-signal representation trade-offs," IEEE Signal Process. Mag. 39, 22–41 (2022).
6. G. Serafino, M. Burla, L. Zhuang, C. Pang, and K.-J. Boller, "High-performance beamforming network based on Si-photonics phase shifters for wideband communications and radar applications," IEEE J. Sel. Top. Quantum Electron. 26, (2020).
7. S. G. Rao and J. D. Cressler, "A D-band reflective-type phase shifter using a SiGe PIN diode resonant load," IEEE Microw. Wireless Compon. Lett. 32, 1191–1194 (2022).
8. H.-C. Chiu, C.-M. Chen, L.-C. Chang, and H.-L. Kao, "A 5-bit X-band GaN HEMT-based phase shifter," Electronics 10, 658 (2021).
9. Y. Yuan, S. J. Chen, and C. Fumeaux, "Varactor-based phase shifters operating in differential pairs for beam-steerable antennas," IEEE Trans. Antennas Propag. 70, 7670–7682 (2022).
10. S. Rahiminejad, S. K. Islam, G. Dadashzadeh, and M. Daneshmand, "A low-loss silicon MEMS phase shifter operating in the 550-GHz band," IEEE Trans. Terahertz Sci. Technol. 11, 477–485 (2021).
11. M. Yasir, S. Bistarelli, A. Cataldo, M. Bozzi, L. Perregrini, and S. Bellucci, "Tunable phase shifter based on few-layer graphene flakes," IEEE Microw. Wireless Compon. Lett. 29, 47–49 (2019).
12. E. A. Casu, A. I. Riikonen, C. C. Chen, and A. P. de los Reyes, "Tunable RF phase shifters based on vanadium dioxide metal–insulator transition," IEEE J. Electron Devices Soc. 6, 965–971 (2018).
13. M. Nickel, M. Koeppe, D. Killat, and R. Jakoby, "Ridge gap waveguide based liquid crystal phase shifter," IEEE Access 8, 77833–77842 (2020).
14. Li-Jing Cheng and Lei Liu, "Optical modulation of continuous terahertz waves towards cost-effective reconfigurable quasi-optical terahertz components," Opt. Express 21, 28657-28667 (2013)
15. A. Kannegulla, M. I. B. Shams, L. Liu, and L.-J. Cheng, "Photo-induced spatial modulation of THz waves: opportunities and limitations," Opt. Express 23, 32098–32112 (2015).
16. Y. Shi, Y. Deng, J. Ren, P. Li, P. Fay, and L. Liu, "Computational analysis of novel high performance optically controlled RF switches for reconfigurable millimeterwave-to-THz circuits," OSA Continuum 4, 2642–2654 (2021).
17. C. Hilsum, "Simple empirical relationship between mobility and carrier concentration," Electron. Lett. 10, 259–260 (1974).
18. I. R. Hooper, E. Khorani, X. Romain, L. E. Barr, T. Niewelt, S. Saxena, A. Wratten, N. E. Grant, J. D. Murphy, and E. Hendry, "Engineering the carrier lifetime and switching speed in Si-based mm-wave photomodulators," J. Appl. Phys. 132, 233102 (2022).
19. I. R. Hooper, N. E. Grant, L. E. Barr, and others, "High efficiency photomodulators for millimeter wave and THz radiation," Sci. Rep. 9, 18304 (2019).
20. M. Rosling, H. Bleichner, M. Lundqvist, and E. Nordlander, "A novel technique for the simultaneous measurement of ambipolar carrier lifetime and diffusion coefficient in silicon," Solid-State Electron. 35(9), 1223–1227 (1992).
21. A. Kannegulla, M. I. B. Shams, L. Liu, and L.-J. Cheng, "Coded-aperture imaging using photo-induced reconfigurable aperture arrays for mapping terahertz beams," IEEE Trans. Terahertz Sci. Technol. 4, 321–327 (2014).
22. M. I. B. Shams, A. Kannegulla, L. Liu, and L.-J. Cheng, "A 740-GHz dynamic two-dimensional beam-steering and forming antenna based on photo-induced reconfigurable Fresnel zone plates," IEEE Trans. Terahertz Sci. Technol. 7, 310–319 (2017).

23. Z. Jiang, M. I. B. Shams, A. Kannegulla, L. Liu, and L.-J. Cheng, “Investigation and demonstration of a WR-4.3 optically controlled waveguide attenuator,” IEEE Trans. Terahertz Sci. Technol. 7, 20–26 (2017).
24. J. Ren, Z. Jiang, P. Fay, J. L. Hesler, C.-Y. E. Tong, and L. Liu, "High-performance WR-4.3 optically controlled variable attenuator with 60-dB range," IEEE Microwave Wireless Compon. Lett. 28(6), 512–514 (2018).
25. P. Li, W. Wu, Y. Shi, Y. Deng, P. Fay, and L. Liu, “Broadband THz switching with extremely low insertion loss and superior isolation,” Proc. IEEE MTT-S Int. Microw. Symp. (IMS), 688–691 (2023).
26. P. Li, W. Wu, Y. Shi, Y. Deng, P. Fay, and L. Liu, “Integrated broadband THz switching using photoconductivity modulation in Si-on-sapphire substrates,” IEEE Trans. Terahertz Sci. Technol. 15, 536–540 (2025).
27. Y. Deng, Y. Shi, P. Li, P. Fay, L.-J. Cheng, and L. Liu, “A cost-effective approach for achieving subwavelength THz imaging using photoinduced coded-apertures on mesa-array structures,” IEEE Trans. Terahertz Sci. Technol. 12, 658–666 (2022).
28. A. Ullah, Y.-C. Wang, S. Yeasmin, Y. Deng, J. Ren, Y. Shi, L. Liu, and L.-J. Cheng, “Reconfigurable photoinduced terahertz wave modulation using hybrid metal–silicon metasurface,” Opt. Lett. 47, 2750–2753 (2022).
29. E. Aydin, M. De Bastiani, and S. De Wolf, “Defect and contact passivation for perovskite solar cells,” Adv. Mater. 31, (2019).
30. A. Pandey, M. Reddeppa, and Z. Mi, “Recent progress on micro-LEDs,” Light Adv. Manuf. 4, 519–542 (2023).
31. I. Cho, Y. C. Sim, M. Cho, Y. Cho, and I. Park, “Monolithic micro light-emitting diode/metal oxide nanowire gas sensor with microwatt-level power consumption,” ACS Sens. 5, 563–570 (2020).
32. E. Carrasco, J. A. Encinar, and M. Barba, "Bandwidth improvement in large reflectarrays by using true-time delay," IEEE Trans. Antennas Propag. 56(8), 2496–2503 (2008).
33. T.-W. Li and H. Wang, “A millimeter-wave fully integrated passive reflection-type phase shifter with transformer-based multi-resonance loads for 360° phase shifting,” IEEE Trans. Circuits Syst. I: Regul. Pap. 65, 1406–1419 (2018).
34. F. Ellinger, T. Djerafi, D. Fritsche, and K. Wu, “Integrated adjustable phase shifters,” IEEE Microw. Mag. 11, 97–108 (2010).